Fluence–Dependent Singlet Exciton Dynamics in Length–Sorted Chirality–Enriched Single–Walled Carbon Nanotubes

4 AUTHORS, INCLUDING:

Jaehong Park
National Renewable Energy Laboratory
12 PUBLICATIONS **184** CITATIONS

SEE PROFILE

Pravas Deria
Southern Illinois University Carbondale
36 PUBLICATIONS **505** CITATIONS

SEE PROFILE

Jean-Hubert Olivier
Duke University
24 PUBLICATIONS **337** CITATIONS

SEE PROFILE

Fluence-Dependent Singlet Exciton Dynamics in Length-Sorted Chirality-Enriched Single-Walled Carbon Nanotubes

Jaehong Park,[†,‡] Pravas Deria,[‡] Jean-Hubert Olivier,[‡] and Michael J. Therien*,[‡]

[†]Department of Chemistry, University of Pennsylvania, 231 South 34th Street, Philadelphia, Pennsylvania 19104-6323, United States

[‡]Department of Chemistry, Duke University, French Family Science Center, 124 Science Drive, Durham, North Carolina 27708-0346, United States

S Supporting Information

ABSTRACT: We utilize individualized, length-sorted (6,5)-chirality enriched single-walled carbon nanotubes (SWNTs) having dimensions of 200 and 800 nm, femtosecond transient absorption spectroscopy, and variable excitation fluences that modulate the exciton density per nanotube unit length, to interrogate nanotube exciton/biexciton dynamics. For pump fluences below 30 μJ/cm^2, transient absorption (TA) spectra of (6,5) SWNTs reveal the instantaneous emergence of the exciton to biexciton transition ($E_{11} \rightarrow E_{11,BX}$) at 1100 nm; in contrast, under excitation fluences exceeding 100 μJ/cm^2, this TA signal manifests a rise time ($\tau_{rise} \sim 250$ fs), indicating that E_{11} state repopulation is required to produce this signal. Femtosecond transient absorption spectroscopic data acquired over the 900−1400 nm spectral region of the near-infrared (NIR) region for (6,5) SWNTs, as a function of nanotube length and exciton density, reveal that over time delays that

exceed 200 fs exciton−exciton interactions do not occur over spatial domains larger than 200 nm. Furthermore, the excitation fluence dependence of the $E_{11} \rightarrow E_{11,BX}$ transient absorption signal demonstrates that relaxation of the E_{11} biexciton state ($E_{11,BX}$) gives rise to a substantial E_{11} state population, as increasing delay times result in a concomitant increase of $E_{11} \rightarrow E_{11,BX}$ transition oscillator strength. Numerical simulations based on a three-state model are consistent with a mechanism whereby biexcitons are generated at high excitation fluences via sequential SWNT ground- and E_{11}-state excitation that occurs within the 980 nm excitation pulse duration. These studies that investigate fluence-dependent TA spectral evolution show that SWNT ground$\rightarrow E_{11}$ and $E_{11} \rightarrow E_{11,BX}$ excitations are coresonant and provide evidence that $E_{11,BX} \rightarrow E_{11}$ relaxation constitutes a significant decay channel for the SWNT biexciton state over delay times that exceed 200 fs, a finding that runs counter to assumptions made in previous analyses of SWNT biexciton dynamical data where exciton−exciton annihilation has been assumed to play a dominant role.

KEYWORDS: Carbon nanotube, femtosecond transient absorption spectroscopy, exciton relaxation dynamics, carbon nanotube length separation
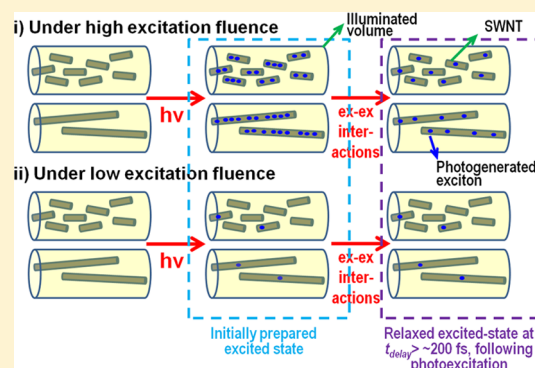
Semiconducting single-walled carbon nanotubes (SWNTs) offer the potential for low-cost photovoltaic materials due to their high aspect ratio, mechanical stability, and substantial carrier mobility.[1−8] The optical excitation of SWNTs produces excitons, Coulomb-interaction bound electron−hole pairs.[9−13] Due to the spatial extent of the SWNT exciton (~1.2−2 nm) relative to typical SWNT dimensions that span length scales of hundreds of nanometers to several micrometers,[9,14,15] multiple excitons can coexist in a single tube;[15−17] exciton−exciton interactions therefore play key roles in the relaxation processes of electronically excited SWNTs produced under high excitation fluence conditions.[10,12,15,17−21] Analyses of fast and ultrafast SWNT excited-state dynamical data acquired under such conditions have therefore considered excited state relaxation mechanisms involving exciton−exciton annihilation, multiple exciton generation, and the formation of biexcitons (excited states derived from the electrostatic interaction of two electron−hole pairs).[12,17,18,20,22] A fundamental understanding

of the nature of these excited states and their dynamics impacts significantly the design of SWNT-based optoelectronic devices. For example, multiple exciton generation in SWNTs[17,23,24] and other nanoscale materials provides opportunities to overcome intrinsic solar energy conversion efficiency limits characteristic of single band gap materials.[25]

Previous work that examined exciton dynamics in low-dimensional materials, such as conjugated polymers/oligomers[26−29] and quantum dots,[10,30−32] suggests that excitons and biexcitons are created simultaneously under high excitation density conditions. In contrast to the large body of work investigating the exciton dynamics of organic/inorganic semiconductors, studies that probe how biexcitons influence exciton dynamics of nanomaterials are rare. In contrast to theoretical

Figure 1. (A) Structural schematic of a polyanionic, conjugated polymer-wrapped SWNT.[41,45−47] (B) Molecular structure of the binaphthalene-based polyanionic semiconducting polymer, *R*−PBN−Ph$_3$.

predictions of stable biexciton state formation in low-dimensional materials,[22,33−40] because biexciton generation typically requires either high excitation densities or sequential excitation (ground state → exciton state → biexciton state), processes such as two-photon excitation or exciton−exciton annihilation often complicate the experimental interrogation of biexciton dynamics. Due to the quantum confinement of electron and hole in pseudo one-dimensional SWNTs, theory predicts the formation of a stable biexciton state, with a binding energy of ∼50−100 meV.[22,37−40] Congruent with this expectation, previous time-resolved transient absorption spectroscopic studies assigned a signal which appears at ∼50−90 meV lower than E$_{11}$ transition as the exciton to biexciton transition (E$_{11}$→E$_{11,BX}$).[19,21,41,42] Despite the experimental precedent for biexciton formation in semiconducting organic materials and nanoparticles, and studies that examine biexciton dynamics in these structures,[26,28,30,31,41,43−46] corresponding detailed information regarding the roles of biexcitons in SWNT excited state dynamics is lacking. We report herein excitation fluence-dependent pump−probe spectroscopic studies of length-sorted (6,5)-chirality enriched SWNTs having dimensions of 200 and 800 nm (Figure 1) that modulate the exciton density per nanotube unit length. These transient absorption spectroscopic studies chronicle SWNT excited dynamics over the NIR spectral domain and show that over time delays that exceed 200 fs: (i) exciton−exciton interactions do not occur over spatial domains larger than 200 nm, and (ii) in contrast to commonly held expectations, diffusion-limited exciton−exciton annihilation does not dominate SWNT biexciton relaxation dynamics.

Figure 2 displays representative linear electronic absorption spectra and NIR transient absorption spectra obtained following E$_{11}$ excitation for individualized (6,5) chirality-enriched SWNTs suspended: (i) in D$_2$O utilizing sodium cholate surfactant (SC−[(6,5) SWNTs]), and (ii) via the efficacy of binaphthalene-based polyanionic semiconducting polymer *R*−PBN−Ph$_3$, which helically wraps[41,45−47] the nanotube surface with periodic and constant morphology (*R*−PBN−Ph$_3$−[(6,5) SWNTs]; Figure 1). These studies, which interrogate the excited state dynamics of chirality enriched tubes,[15,17,20,41,48] enable direct identification of SWNT transient absorption spectral signatures, and contrast earlier SWNT excited state dynamical studies that manifest complications presented by broad spectral domain transient bleaching signatures characteristic of heterogeneous SWNT samples comprising multiple chiralities. Congruent with

Figure 2. (A) Electronic absorption spectra of (6,5) SWNTs suspended in D$_2$O utilizing sodium cholate (SC) surfactant (SC−[(6,5) SWNTs], black) and (6,5) SWNTs suspended in D$_2$O via helical wrapping by the *R*−PBN−Ph$_3$ polymer (*R*−PBN−Ph$_3$−[(6,5) SWNTs]); note that these *R*−PBN−Ph$_3$−[(6,5) SWNT] samples were prepared from chirality-enriched (6,5) SWNTs having average lengths of ∼0.8 μm (red) and ∼0.2 μm (green) (see Supporting Information). (B) Representative transient absorption spectra obtained for SC−[(6,5) SWNTs] at the time delays noted. Experimental conditions: λ$_{ex}$ = 980 nm; solvent = D$_2$O; temperature = 20 °C; magic angle polarization; excitation pump fluence = 29.2 μJ/cm^2.

previous studies,[15,20,41] transient absorption spectra shown in Figure 2 are dominated by the ground-state bleaching band in the E$_{11}$ spectral region; note that, in the 900−1400 nm spectral region of the NIR, three transient absorption (TA) bands are also observed that are lower in energy than the E$_{11}$ bleach. A TA band lying at the red edge of the E$_{11}$ bleach (TA1) is evident at t_{delay} = 300 fs; this transient decays with a time constant of ∼34 ps (Figure S8). Given its transition energy and the fact that a typical E$_{11}$ state lifetime is on the order of tens of picoseconds, TA1 has been assigned previously to an exciton to biexciton transition (E$_{11}$→E$_{11,BX}$);[19,22] the oscillator strength of this transition is thus proportional to the E$_{11}$ exciton population. Note that although the TA1 transition energy (∼1100 nm; ∼1.13 eV) matches approximately the emission energy (1.12 eV) of the (6,5) phonon sideband,[49] the fact that TA1 is a transient absorptive (positive) signal precludes the
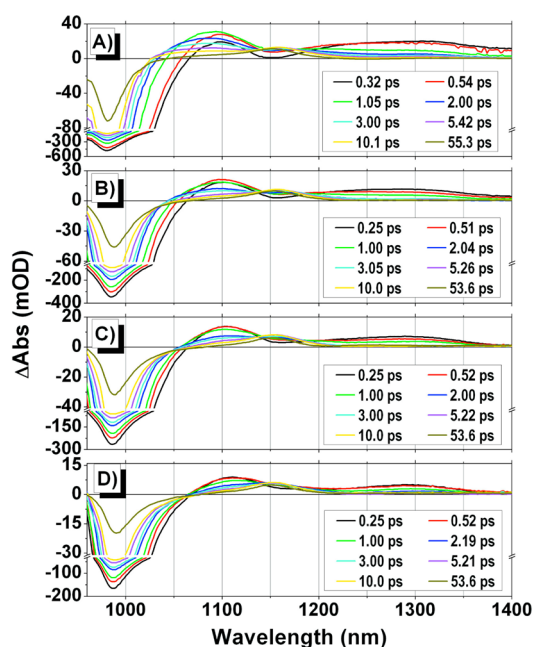
Figure 3. Representative fluence-dependent transient absorption spectra obtained for SC−[(6,5) SWNTs] at the time delays noted. Experimental conditions: λ_{ex} = 980 nm; solvent = D$_2$O; temperature = 20 °C; magic angle polarization; excitation pump fluences: (A) 1714 μJ/cm^2, (B) 448.7 μJ/cm^2, (C) 112.8 μJ/cm^2, (D) 29.2 μJ/cm^2; following all of these pump−probe transient absorption experiments, electronic absorption spectra verified that these SC−[(6,5) SWNT] samples were robust.

possibility that TA1 derives from (6,5) phonon sideband emission. Note that TA1 is evident at time delays <100 fs when an excitation fluence of ~30 μJ/cm^2 is utilized (Figure 3D); in contrast, in experiments that utilize pump fluences exceeding ~100 μJ/cm^2, TA1 is observed to *exhibit a fluence-dependent rise*, which has not been observed previously (vide infra).

As underscored in Figure 2, another TA band (TA2) at ~1160 nm is evident at t_{delay} > 10 ps. Previous transient dynamical studies[41] confirm that TA2 corresponds to a T$_1$→T$_n$ (^{3}E$_{11}$→^{3}E$_{nn}$) transition[41,50] and demonstrate that the (6,5) SWNT ^{3}E$_{11}$ state: (i) possesses a microsecond lifetime ($\tau_T \approx$ 10−15 μs), (ii) manifests ^{3}O$_2$ quenching dynamics reminiscent of those determined for conjugated aromatic hydrocarbon excited triplet states, and (iii) is populated via picosecond time-scale intersystem crossing dynamics.[41,51] Furthermore, the transition energy and full-width at half-maximum of TA2 (the ^{3}E$_{11}$→^{3}E$_{nn}$ absorptive signal) do not vary with the nature of SWNT surfactant or solvent dielectric. Likewise, the fact that TA2 can be observed even in pump−probe transient absorption spectroscopic experiments carried out using E$_{11}$ excitation and extremely low excitation fluences that generate < ~0.8 excitons per ~700 nm nanotube (SI; Figure S5), where exciton−exciton interactions are negligible, coupled with the significant (6,5) SWNT E$_{11}$-exciton binding energy of ~0.4 eV,[9,10] is congruent with: (i) suppression of a significant hot exciton population and corresponding hot-exciton derived dissociation products and (ii) negligible exciton−exciton annihilation mediated generation of exciton-dissociation products such as polarons, which therefore cannot serve as the genesis of the state that gives rise to TA2. In addition, a broad TA band (TA3) is evident at the earliest possible time delays over the 1200−1400 nm spectral window; note that the

state that gives rise to this transition possesses a lifetime of ~0.7 ps. These NIR transient absorptive features for (6,5) enriched SWNTs, observed over the 900−1400 nm spectral domain, thus indicate that at least three different SWNT excited-state species are produced under these excitation conditions, as the states that give rise to transient signals TA1, TA2, and TA3 manifest distinctly disparate relaxation kinetics. While numerous studies have been reported that examine SWNT exciton relaxation dynamics using pump−probe spectroscopy,[12,15,17−21,52,53] only a few of these studies[15,20,21] interrogate transient absorptive signals that directly track the E$_{11}$ exciton population. In this study, we utilize individualized, length-sorted (6,5)-chirality enriched single-walled carbon nanotubes (SWNTs) having dimensions of 200 and 800 nm, femtosecond transient absorption spectroscopy, and variable excitation fluences that modulate the exciton density per nanotube unit length, to interrogate nanotube exciton/biexciton dynamics and ascertain why the E$_{11}$ state population that gives rise to this transition centered at 1100 nm manifests extreme sensitivity to the excitation pump fluence.

Figures 3 and S6 display fluence-dependent transient absorption spectral evolution following E$_{00}$→E$_{11}$ excitation of SC−[(6,5) SWNTs]. In these experiments, the pump fluence was varied from 6.5 to 1714 μJ/cm^2; following all of these pump−probe transient absorption experiments, electronic absorption spectra verified that these SC−[(6,5) SWNT] samples were robust. Figure 3D shows transient absorption spectral data acquired using an excitation pump fluence of 29.2 μJ/cm^2; note the instantaneous emergence of TA1, congruent with the fact that this transition originates from the E$_{11}$ state.[50] In contrast, Figure 3A−C, which displays transient absorption spectral data acquired using excitation fluences exceeding ~100 μJ/cm^2, highlights that, while TA1 is evident instantaneously, its oscillator strength progressively increases over the earliest delay times: a diminished early time E$_{11}$ population, relative to that evident at low excitation pump fluence, recovers with increasing time delays. Note that Figure S7, which displays normalized transient absorption spectra acquired between 0.12 ps < t_{delay} < 0.44 ps, where the delayed emergence of TA1 is observed, verifies that the observed TA1 rise time is not a consequence of spectral broadening of the E$_{11}$ bleaching band. Figure 4A compares fluence-dependent TA1 signal intensities as a function of time. For excitation fluences exceeding 113 μJ/cm^2, the transient signal at 1110 nm exhibits an increase in oscillator strength during the initial 1 ps following its instantaneous emergence after excitation, contrasting analogous data acquired for excitation pump fluences at or below 29 μJ/cm^2. While multiexponential fitting of the transient signal observed at ~1100 nm for SC−[(6,5) SWNTs] reveals a fluence-independent rise time constant of ~250 fs, note that the amplitude of this 250 fs rising component increases with increasing excitation fluence (Figure S8). While it has been long appreciated that under high fluence conditions two-photon SWNT excitation (E$_{00}$ + 2$h\nu$ → E$_{nn}$) can take place, E$_{nn}$→E$_{11}$ relaxation dynamics occur on a sub 100 fs time scale,[53,54] which is significantly faster than the time constant (~250 fs) for the TA1 rising component evident in Figure 4A for high fluence E$_{00}$→E$_{11}$ excitation at 980 nm. Figure 4B−C displays transient signal decays at 985 and 1110 nm, shown normalized at t_{delay} = 2 ps, for time delays ranging up through 500 ps. These data demonstrate that, while the rise amplitude of the E$_{11}$ state is pump-fluence dependent, once E$_{11}$ state production ceases, the observed E$_{11}$ state relaxation dynamics
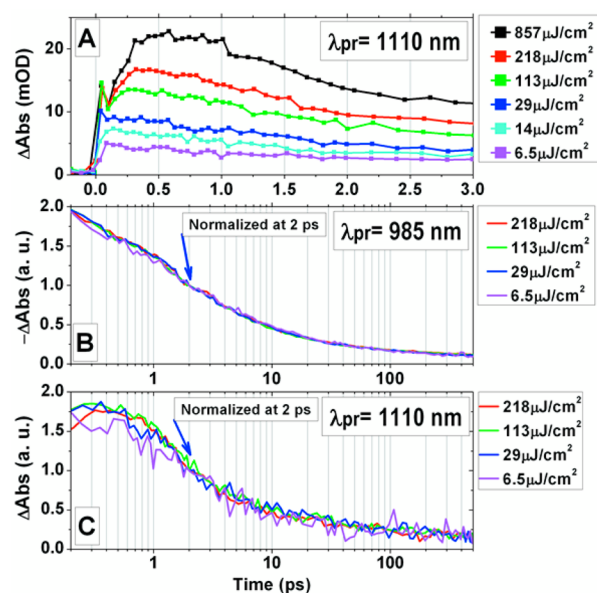
Figure 4. (A) Comparative fluence-dependent SC−[(6,5) SWNT] transient absorption signal intensities as a function of time for the $E_{11} \rightarrow E_{11,BX}$ transition (TA1, Figure 2), determined at 1110 nm, following E_{11} excitation and recorded over time delays ranging up to 3 ps. (B, C) Excitation fluence-dependence of: (B) the ground→E_{11} bleaching signal intensity at 985 nm, and (C) the TA1 signal intensity at 1110 nm, following E_{11} excitation (λ_{ex} = 980 nm) for SC−[(6,5) SWNTs] recorded over time delays ranging up to 500 ps; these data are displayed normalized at the respective signal intensities recorded at t_{delay} = 2 ps. Experimental conditions: solvent = D_2O; temperature = 20 °C; magic angle polarization; probe wavelengths (λ_{pr}) are noted in the figure panel insets; following all of these pump−probe transient absorption experiments, electronic absorption spectra verified that these SC−[(6,5) SWNT] samples were robust.

are fluence-independent. These results run counter to expectations for an excited-state relaxation pathway dominated by diffusion-limited exciton−exciton annihilation (EEA), where increased exciton densities that derive from augmented pump fluences would result in increasingly faster ground state recovery dynamics. Furthermore, a diffusion-limited EEA process should manifest a characteristic time-dependent annihilation rate constant:[55,56] such characteristic time-dependent dynamics are not evident in these data.

To probe the extent to which SWNT exciton density impacts relaxation dynamics, length-sorted (6,5) SWNT samples were utilized. Among the reported SWNT length-sorting techniques,[16,57−60] HPLC-based size exclusion chromatography (SEC)[16,58] is particularly attractive as it is cost-effective, scalable, and assures reproducibility. Previous work from our group has demonstrated that highly charged aryleneethynylene polymers exfoliate, individualize, and disperse SWNTs via a single chain helical wrapping mechanism,[41,45−47,61−63] providing robust, polymer-SWNT superstructures in which nanotubes retain established semiconducting and conducting properties (Figure 1A).[41,45] The preparation of ionic semiconducting polymer-wrapped (6,5) SWNTs utilizes density gradient (DG) separated SC−[(6,5) SWNTs].[41,47,63] In this study, a chiral binaphthalene (PBN)-based semiconducting polymer, R−PBN−Ph$_3$, was utilized to wrap (6,5) SWNTs prior to a SEC-based length sorting process; the PBN-based helical polymer provides high recovery of (6,5) SWNTs (>95%) following SEC separation. AFM experiments probed the length

and structure of these length-sorted R−PBN−Ph$_3$−[(6,5) SWNT] fractions; statistical analyses of these AFM data (Supporting Information) establish average (6,5) SWNT lengths of ∼0.75 ± 0.1 μm and ∼0.17 ± 0.01 μm for the respective l = 0.8 μm and l = 0.2 μm R−PBN−Ph$_3$−[(6,5) SWNT] samples utilized in this investigation (Figure S10B,E; Figures S9−11). Electronic absorption spectral data (Figure 2) confirm that the l = 0.2 μm R−PBN−Ph$_3$−[(6,5) SWNT] sample retains intrinsic nanotube E_{11} and E_{22} transitions. Previous data that investigated highly charged, aryleneethynylene polymers designed to helically wrap SWNTs as well as feature frontier orbital energy levels energetically displaced from the nanotube valence and conduction bands demonstrated that SWNT excited-state relaxation dynamics are not perturbed by the helical polymer wrapping of the SWNT surface relative to those elucidated for benchmark, surfactant-dispersed SWNT samples.[41,45] Similarly, fluence-dependent pump−probe transient absorption spectroscopic experiments demonstrate that these R−PBN−Ph$_3$−[(6,5) SWNT] samples exhibit ground→E_{11} bleaching recovery dynamics and fluence-dependent rise times for the $E_{11} \rightarrow E_{11,BX}$ transition (TA1) identical to that determined for SC−[(6,5) SWNTs] (Figure S12), indicating that the R−PBN−Ph$_3$ polymer does not perturb SWNT E_{11} state relaxation dynamics.

These length-sorted (6,5) SWNT samples (l = 0.8 μm and l = 0.2 μm R−PBN−Ph$_3$−[(6,5) SWNTs]) enable examination of the spatial extent of exciton−exciton interactions. Scheme 1 depicts possible exciton−exciton interactions as a function of SWNT length, exciton diffusion length, and excitation fluence and provides a simple framework with which to discuss fluence-dependent ground→E_{11} bleaching signal intensity data acquired for the 0.8 μm and 0.2 μm long R−PBN−Ph$_3$−[(6,5) SWNT] samples (Figure 5). Like the Figure 4 data that probe the excitation fluence and time dependence of the $E_{11} \rightarrow E_{11,BX}$ transient absorption and ground→E_{11} bleaching signal intensities for SC−[(6,5) SWNTs], analogous data acquired for length-sorted R−PBN−Ph$_3$−[(6,5) SWNTs] demonstrate that EEA dynamics are not evident over time delays that exceed ∼200 fs (Figure 5), as ground→E_{11} bleaching recovery dynamics are clearly fluence-independent. Note that, if the nanotube length scale sampled by an exciton (the diffusion length) is much larger than ∼0.2 μm, most excitons will collide during the duration of the laser excitation pump pulse (Scheme 1A). In this case, under high excitation fluence conditions (Scheme 1A-i), the instantaneous exciton density per nanotube unit length is high. Rapid EEA that occurs within the excitation pulse duration will leave ∼1 exciton per tube at time delays exceeding 200 fs; shorter SWNT samples (l = 0.2 μm) would thus be predicted to exhibit an exciton population ∼4 times higher relative to longer SWNT samples (l = 0.8 μm) for an equivalent nanotube mass. In contrast, for the case where the exciton diffusion length exceeds ∼0.2 μm and the excitation fluence is low (Scheme 1A-ii), EEA does not play a significant role in suppressing the exciton population, and equivalent masses of 0.2 μm and 0.8 μm long SWNTs will possess a similar number of excitons. (Note that the diffusion constant of carbon nanotubes in aqueous suspension has been determined to be 0.3−6 × 10^{-8} cm^2/s,[64] while the SWNT exciton diffusion constant has been estimated to be on the order of 0.1−10 cm^2/s;[15,60] in these experiments, the possibility of intertube exciton−exciton interactions are thus precluded.) If the hypothesis that the exciton diffusion length is much larger than ∼0.2 μm is correct, and the assumption that any exciton−

Scheme 1. Schematic Description of SWNT Exciton–Exciton Interactions as a Function of Nanotube Length, Exciton Diffusion Length, and Excitation Fluence[a]

A) If exciton-exciton interactions occur over distances longer than ~200 nm:
i) Under high excitation fluence

ii) Under low excitation fluence
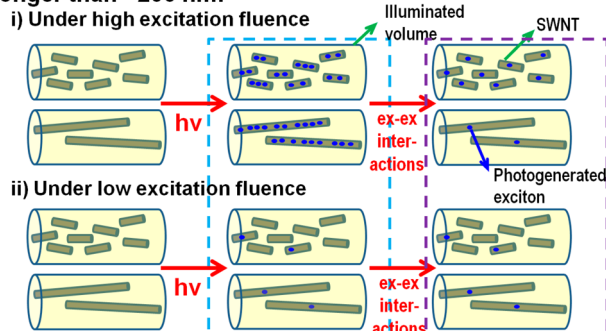
B) If exciton-exciton interactions occur over distances shorter than ~200 nm:
i) Under high excitation fluence

ii) Under low excitation fluence
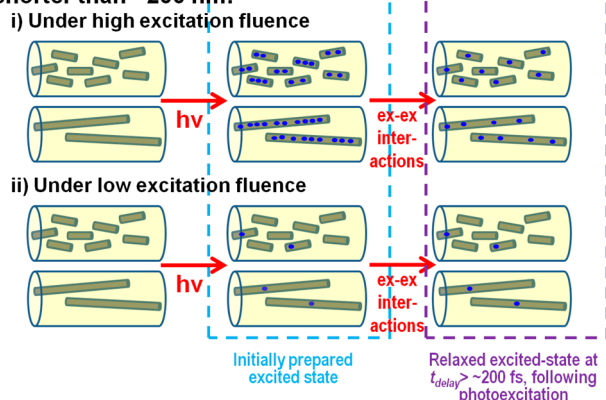
[a]Yellow cylinders represent the illuminated volume of the SWNT sample, while the brown cylinders represent 0.2 μm and 0.8 μm long length-sorted SWNTs. Blue circles represent photogenerated excitons.

Figure 5. (A) Comparative fluence-dependent ground→E_{11} bleaching signal intensities, normalized at t_{delay} = 2 ps, as a function of time for $R-PBN-Ph_3-[$(6,5) SWNTs$]$ having average nanotube lengths of ~0.2 μm (solid line) and ~0.8 μm (dashed line); see Supporting Information. (B) Plot of the ground→E_{11} bleaching peak intensities obtained for $R-PBN-Ph_3-[$(6,5) SWNT$]$ samples having average nanotube lengths of ~0.2 μm (black) and ~0.8 μm (red) as a function of the excitation pump fluence. Experimental conditions: solvent = D_2O; λ_{ex} = 1000 nm; λ_{pr} = 1001 nm; temperature = 20 °C; magic angle polarization.

exciton interactions are completed within the pump pulse duration (~200 fs) of these experiments is valid, a plot of the ground→E_{11} transient bleach signal intensity as a function of excitation fluence should reveal that the bleaching signal intensity observed for the 0.2 μm long SWNT sample eventually surpasses that observed for 0.8 μm long SWNTs for some critical fluence and at an identical nanotube mass (Scheme 1A) and that the steepness of a plot of bleach signal intensity vs excitation fluence for 0.2 μm long SWNTs should exceed that of the 0.8 μm long SWNT sample.

On the other hand, if the exciton diffusion length is much less than ~0.2 μm, only excitons generated in close proximity can interact (Scheme 1B). For such a case, a plot of the E_{11} bleach signal intensity as a function of excitation fluence should reveal identical dependences for the 0.2 μm and 0.8 μm long SWNT samples having identical nanotube masses. Figure 5A displays ground→E_{11} bleaching signal intensities recorded as a function of time for 0.2 μm and 0.8 μm long $R-PBN-Ph_3-[$(6,5) SWNT$]$ samples, normalized at t_{delay} = 2 ps [the time delay at which no rising component is evident at any excitation fluence utilized in this study (Figure 4A, 6A)]; these data indicate that for time delays ranging up through 1000 ps, the observed E_{11} bleaching intensity decay dynamics are observed to be fluence-independent, similar to the data chronicled in Figure 4B for $SC-[$(6,5) SWNTs$]$ having a heterogeneous distribution of length scales. Figure 5B plots the ground→E_{11}
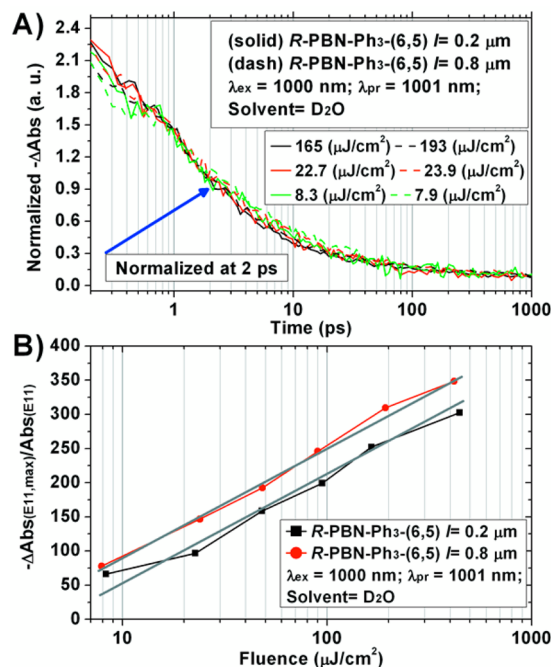
bleaching signal intensities as a function of excitation fluence for these 0.2 μm and 0.8 μm long $R-PBN-Ph_3-[$(6,5) SWNT$]$ samples. These data indicate identical dependences of the ground→E_{11} bleaching signal intensity as a function of excitation fluence for 0.2 μm and 0.8 μm long $[$(6,5) SWNTs$]$ and are consistent with an exciton model in which: (i) the spatial extent of E_{11} exciton–exciton interactions of (6,5) SWNTs is less than ~0.2 μm, and (ii) exciton–exciton interactions are negligible at time delays exceeding 2 ps (Scheme 1B).[15,65]

The exciton density per 100 nm SWNT unit length can be calculated for these $R-PBN-Ph_3-[$(6,5) SWNT$]$ and $SC-[$(6,5) SWNT$]$ samples based on pump-fluence-dependent transmittance measurements at E_{11} (Supporting Information), assuming an absorptive cross-section σ_C = 7 × 10^{-18} cm^2 for (6,5) SWNTs.[15,16] Note that the transmittance values determined for these nanotube samples ($SC-[$(6,5) SWNTs$]$ and $R-PBN-Ph_3-[$(6,5) SWNTs$]$) remain constant through excitation fluences ranging up to ~20 μJ/cm^2 (Figure S13), indicating that the exciton density increases linearly with excitation fluence; note that, for excitation fluences of 6.5 and 29 μJ/cm^2, ~1.8 and ~3.8 excitons are respectively generated per 100 nm in (6,5) SWNTs. In contrast, for 113 μJ/cm^2 and 857 μJ/cm^2 excitation fluences, where the rise of the E_{11}→$E_{11,BX}$ transition is clearly evident, ~5.7 and ~7.7 excitons, respectively, are created per 100 nm (Figure 4A). Given the approximate SWNT exciton size (<2 nm),[9,14,15] it is thus not surprising that at a 6.5 μJ/cm^2 excitation fluence (~1.8 excitons per 100 nm tube), a biexciton state is less likely to be generated
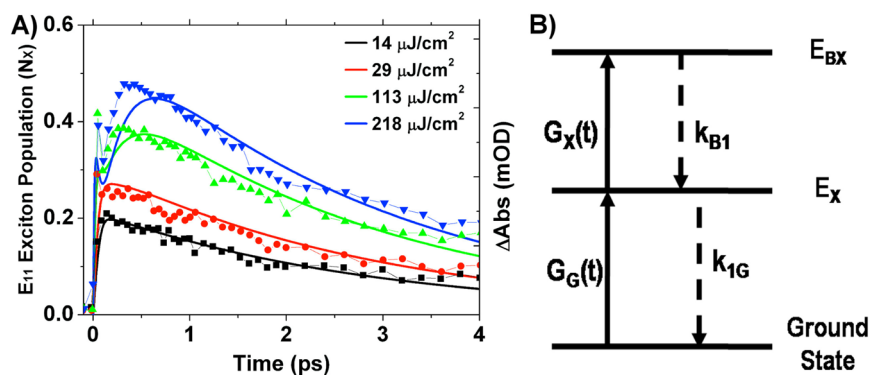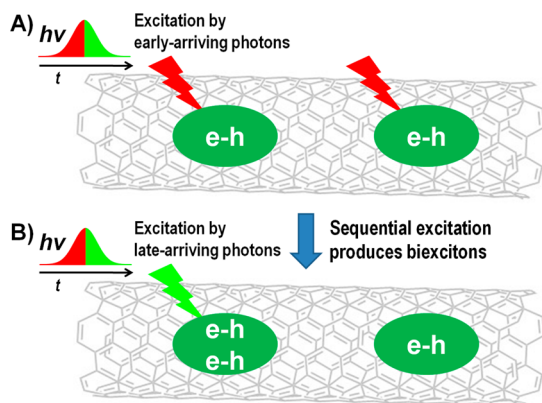
Figure 6. (A) Comparison of experimental (symbols) and numerical simulation (solid lines) data that chronicle the E_{11} exciton population as functions of time and excitation pump fluence. See eqs 1−2. Experimental data displayed correspond to that acquired for SC−[(6,5) SWNTs]; experimental conditions: λ_{ex} = 980 nm; λ_{pr} = 1110 nm; solvent = D_2O; temperature = 20 °C; magic angle polarization. (B) Diagrammatic representation of the three-state model utilized in the numerical simulation.

within the duration of the pump pulse (Figure 4A) than for cases where the pump fluence exceeds ∼100 $\mu J/cm^2$ (∼6 or more excitons per 100 nm tube, Figure 4A). The generation of biexcitons at high pump fluences results in delayed formation of the TA1 signal, as sequential excitation produces the $E_{11,BX}$ state at the expense of the E_{11} (Scheme 2). These exciton density

Scheme 2. Schematic Description of Sequential Ground→ E_{11} and E_{11}→$E_{11,BX}$ Excitations Occurring within the Pump Pulse Duration[a]

[a](A) Photoexcitation by early arriving photons at high excitation fluence generates multiple excitons in a single carbon nanotube via ground→E_{11} excitation. (B) When high excitation fluences are utilized, the probability of sequential ground→E_{11} and E_{11}→$E_{11,BX}$ excitation occurring within the pump pulse increases, producing biexcitons; this description is consistent with a model previously described by Klimov.[28]

calculations, as well as analysis of the excitation fluence- and time-dependent evolution of the E_{11}→$E_{11,BX}$ transition oscillator strength (TA1) provide compelling evidence that the ground→E_{11} and E_{11}→$E_{11,BX}$ transitions are coresonant and that significant E_{11} state repopulation occurs via biexciton state ($E_{11,BX}$) relaxation. Throughout these studies that probe the excitation fluence dependence of SWNT biexciton dynamics, ground state Raman spectroscopy was employed to quantify any irradiation-induced defects in these samples (Figure S15), as it has been established that SWNT D band intensity (1250− 1450 cm^{-1}) correlates with the extent of SWNT defect sites.[66,67] Note that no D band spectral intensity was observed either prior to or following these experiments, indicating that,

even following prolonged interrogation at high fluence, no measurable defect site population was generated.

To understand the pump-fluence dependence of SWNT biexciton and exciton dynamics in more detail, a numerical simulation of the time dependence of the E_{11} state population was carried out, using an approach described by Klimov[28] in an analysis of the excitation intensity dependence of biexciton dynamics in π-conjugated systems. In this model, biexciton generation is assumed to occur within the pump pulse duration via sequential ground→E_{11} and E_{11}→$E_{11,BX}$ excitation. The time evolution of exciton and biexciton populations is described using the equations below; note that due to saturable absorption effects at high pump fluences, these numerical simulations apply a fluence-dependent correction factor (see Supporting Information).

$$\frac{dN_X}{dt} = G_G(t)N_G - G_X(t)N_X - k_{1G}N_X + k_{B1}N_{BX} \tag{1}$$

$$\frac{dN_{BX}}{dt} = G_X(t)N_X - k_{B1}N_{BX} \tag{2}$$

Here, the exciton generation rate from the ground state, $G_G(t)$, depends explicitly on time and is defined as a 150 fs fwhm Gaussian function, characteristic of the pump pulse used in these pump−probe experiments. The magnitude of the Gaussian pulse, $G_G(t)$, is directly proportional to the experimental pump fluences. Likewise, the biexciton generation rate from the exciton state, $G_X(t)$, is also related to these factors (see Supporting Information), k_{1G} is the E_{11} relaxation rate to the ground state, k_{B1} is the biexciton relaxation rate, N_X is the population of E_{11} excitons, N_{BX} represents the population of biexcitons, and N_G denotes the ground-state population.

Figure 6A compares experimental and numerical simulation data that chronicle the E_{11} exciton population as functions of time and excitation pump fluence based on this three-state model (eqs 1−2; Figure 6B); in this analysis, the biexciton relaxation rate is obtained from the rise time constant (∼250 fs) of TA1, while k_{1G} was determined from a corresponding biexponential fit of the 1100 nm transient signal. Note that the data derived from this numerical simulation closely mirror the transient absorption experimental results. Further, this simulation accounts for the delayed emergence of the E_{11} population (N_X) as the excitation fluence increases, and the prominence of the observed valley evident at a time delay of ∼0.1 ps (Figure 6A) which tracks the larger biexciton

populations that result from increasingly probable sequential ground→E_{11} and E_{11}→$E_{11,BX}$ excitations that occur within the time domain of the pump pulse as excitation fluence increases. These experimental and simulational results indicate that the $E_{11,BX}$→E_{11} transition constitutes a significant relaxation channel for the SWNT biexciton state.

In summary, SWNT exciton dynamics were interrogated through the agency of length-sorted (6,5) chirality-enriched SWNTs, femtosecond pump−probe transient absorption spectroscopic methods, and variable excitation pump fluences. For pump fluences below 30 μJ/cm^2, transient absorption spectra of (6,5) SWNTs suspended in D_2O reveal the instantaneous emergence of a transient signal at 1100 nm [the exciton to biexciton transition (E_{11}→$E_{11,BX}$)], consistent with the fact that it derives from the E_{11} state; in contrast, when excitation pump fluences exceeding 100 μJ/cm^2 are utilized, the transient signal at 1100 nm manifests a rise time with a time constant of ∼250 fs, following its instantaneous emergence, indicating that repopulation of the E_{11} state is responsible for the rising signal intensity at this wavelength. Femtosecond transient absorption spectroscopic data acquired over the 900−1400 nm spectral region of the NIR for (6,5) SWNTs, as a function of nanotube length and exciton density, reveal that *over time delays that exceed 200 fs* that exciton−exciton interactions do not occur over spatial domains larger than 200 nm. Furthermore, the excitation fluence dependence of the E_{11}→$E_{11,BX}$ transient absorption signal demonstrates that relaxation of the E_{11} biexciton state ($E_{11,BX}$) gives rise to a substantial E_{11} state population, as increasing delay times result in a concomitant increase of E_{11}→$E_{11,BX}$ transition oscillator strength. Numerical simulation of these data based on a three-state model is consistent with a mechanism whereby biexcitons are generated at high pump fluences via sequential ground→E_{11} and E_{11}→$E_{11,BX}$ excitations that occur within the duration of the 980 nm pump pulse. These experiments that monitor NIR transient absorption spectral evolution as a function of exciton density and nanotube length over time delays exceeding 200 fs, provide evidence that: (i) ground→E_{11} and E_{11}→$E_{11,BX}$ excitations are coresonant, and (ii) $E_{11,BX}$→E_{11} relaxation constitutes a significant decay channel for the SWNT biexciton state, a finding that runs counter to assumptions made in previous analyses of SWNT biexciton dynamical data in which diffusion-limited exciton−exciton annihilation has been assumed to play a dominant role.

ASSOCIATED CONTENT

Ⓢ Supporting Information

Synthetic procedures, characterization data (^{1}H NMR, ^{13}C NMR, mass spectra, IR, and XPS), sample preparation details, additional transient spectroscopic experimental data, exciton density calculations, and details regarding the numerical simulations. This material is available free of charge via the Internet at http://pubs.acs.org.

AUTHOR INFORMATION

Corresponding Author

*Address: 5330 French Family Science Center, 124 Science Drive, Duke University, Box 90346, Durham, North Carolina 27708-0346. E-mail: michael.therien@duke.edu.

Notes

The authors declare no competing financial interest.

REFERENCES

(1) Ago, H.; Petritsch, K.; Shaffer, M. S. P.; Windle, A. H.; Friend, R. H. *Adv. Mater.* **1999**, *11*, 1281−1285.

(2) Bhattacharyya, S.; Kymakis, E.; Amaratunga, G. A. J. *Chem. Mater.* **2004**, *16*, 4819−4823.

(3) Sgobba, V.; Rahman, G. M. A.; Guldi, D. M.; Jux, N.; Campidelli, S.; Prato, M. *Adv. Mater.* **2006**, *18*, 2264−2269.

(4) Geng, J.; Zeng, T. *J. Am. Chem. Soc.* **2006**, *128*, 16827−16833.

(5) Avouris, P.; Chen, Z.; Perebeinos, V. *Nat. Nanotechnol.* **2007**, *2*, 605−615.

(6) Guo, X.; Xiao, S.; Myers, M.; Miao, Q.; Steigerwald, M. L.; Nuckolls, C. *Proc. Natl. Acad. Sci. U.S.A.* **2009**, *106*, 691−696.

(7) Bindl, D. J.; Safron, N. S.; Arnold, M. S. *ACS Nano* **2010**, *4*, 5657−5664.

(8) Schnorr, J. M.; Swager, T. M. *Chem. Mater.* **2011**, *23*, 646−657.

(9) Wang, F.; Dukovic, G.; Brus, L. E.; Heinz, T. F. *Science* **2005**, *308*, 838−841.

(10) Scholes, G. D.; Rumbles, G. *Nat. Mater.* **2006**, *5*, 683−696.

(11) Dresselhaus, M. S.; Dresselhaus, G.; Saito, R.; Jorio, A. *Annu. Rev. Phys. Chem.* **2007**, *58*, 719−747.

(12) Carlson, L. J.; Krauss, T. D. *Acc. Chem. Res.* **2008**, *41*, 235−243.

(13) Kilina, S.; Tretiak, S.; Doorn, S. K.; Luo, Z.; Papadimitrakopoulos, F.; Piryatinski, A.; Saxena, A.; Bishop, A. R. *Proc. Natl. Acad. Sci. U.S.A.* **2008**, *105*, 6797−6802.

(14) Spataru, C. D.; Ismail-Beigi, S.; Benedict, L. X.; Louie, S. G. *Phys. Rev. Lett.* **2004**, *92*, 77402.

(15) Lüer, L.; Hoseinkhani, S.; Polli, D.; Crochet, J.; Hertel, T.; Lanzani, G. *Nat. Phys.* **2009**, *5*, 54−58.

(16) Fagan, J. A.; Simpson, J. R.; Bauer, B. J.; Lacerda, S. H. D. P.; Becker, M. L.; Chun, J.; Migler, K. B.; Walker, A. R. H.; Hobbie, E. K. *J. Am. Chem. Soc.* **2007**, *129*, 10607−10612.

(17) Wang, S.; Khafizov, M.; Tu, X.; Zheng, M.; Krauss, T. D. *Nano Lett.* **2010**, *10*, 2381−2386.

(18) Ma, Y.-Z.; Valkunas, L.; Dexheimer, S. L.; Bachilo, S. M.; Fleming, G. R. *Phys. Rev. Lett.* **2005**, *94*, 157402.

(19) Ma, Y.-Z.; Valkunas, L.; Dexheimer, S. L.; Fleming, G. R. *Mol. Phys.* **2006**, *104*, 1179−1189.

(20) Zhu, Z.; Crochet, J.; Arnold, M. S.; Hersam, M. C.; Ulbricht, H.; Resasco, D.; Hertel, T. *J. Phys. Chem. C* **2007**, *111*, 3831−3835.

(21) Styers-Barnett, D. J.; Ellison, S. P.; Mehl, B. P.; Westlake, B. C.; House, R. L.; Park, C.; Wise, K. E.; Papanikolas, J. M. *J. Phys. Chem. C* **2008**, *112*, 4507−4516.

(22) Pedersen, T. G.; Pedersen, K.; Cornean, H. D.; Duclos, P. *Nano Lett.* **2005**, *5*, 291−294.

(23) Nozik, A. J. *Nat. Nanotechnol.* **2009**, *4*, 548−549.

(24) Gabor, N. M.; Zhong, Z.; Bosnick, K.; Park, J.; McEuen, P. L. *Science* **2009**, *325*, 1367−1371.

(25) Shockley, W.; Queisser, H. J. *J. Appl. Phys.* **1961**, *32*, 510−519.

(26) Takeuchi, S.; Masuda, T.; Kobayashi, T. *J. Chem. Phys.* **1996**, *105*, 2859−2874.

(27) Kranzelbinder, G.; Nisoli, M.; Stagira, S.; De Silvestri, S.; Lanzani, G.; Mullen, K.; Scherf, U.; Graupner, W.; Leising, G. *Appl. Phys. Lett.* **1997**, *71*, 2725−2727.

(28) Klimov, V. I.; McBranch, D. W.; Barashkov, N.; Ferraris, J. *Phys. Rev. B: Condens. Matter* **1998**, *58*, 7654−7662.

(29) Labastide, J. A.; Baghgar, M.; McKenna, A.; Barnes, M. D. *J. Phys. Chem. C* **2012**, *116*, 23803−23811.

(30) Klimov, V. I.; Ivanov, S. A.; Nanda, J.; Achermann, M.; Bezel, I.; McGuire, J. A.; Piryatinski, A. *Nature* **2007**, *447*, 441−446.

(31) Cooney, R. R.; Sewall, S. L.; Sagar, D. M.; Kambhampati, P. *Phys. Rev. Lett.* **2009**, *102*, 127404.

(32) Kambhampati, P. *Acc. Chem. Res.* **2011**, *44*, 1−13.

(33) Guo, F.; Chandross, M.; Mazumdar, S. *Phys. Rev. Lett.* **1995**, *74*, 2086−2089.

(34) Gallagher, F. B.; Spano, F. C. *Phys. Rev. B* **1996**, *53*, 3790−3803.

(35) Mazumdar, S.; Guo, F.; Meissner, K.; Fluegel, B.; Peyghambarian, N.; Kuwata-Gonokami, M.; Sato, Y.; Ema, K.; Shimano, R.; Tokihiro, T.; Ezaki, H. *J. Chem. Phys.* **1996**, *104*, 9292−9296.

(36) Gao, K.; Xie, S.; Yin, S.; Liu, D. *Org. Electron.* **2012**, *13*, 784−788.

(37) Kammerlander, D.; Prezzi, D.; Goldoni, G.; Molinari, E.; Hohenester, U. *Phys. Rev. Lett.* **2007**, *99*, 126806.

(38) Bondarev, I. V. *Phys. Rev. B* **2011**, *83*, 153409.

(39) Watanabe, K.; Asano, K. *Phys. Rev. B* **2011**, *83*, 115406.

(40) Rønnow, T. F.; Pedersen, T. G.; Partoens, B. *Phys. Rev. B* **2012**, *85*, 045412.

(41) Park, J.; Deria, P.; Therien, M. J. *J. Am. Chem. Soc.* **2011**, *133*, 17156−17159.

(42) Gao, B.; Hartland, G. V.; Huang, L. *ACS Nano* **2012**, *6*, 5083−5090.

(43) Leng, J. M.; Jeglinski, S.; Wei, X.; Benner, R. E.; Vardeny, Z. V.; Guo, F.; Mazumdar, S. *Phys. Rev. Lett.* **1994**, *72*, 156−159.

(44) Stone, K. W.; Gundogdu, K.; Turner, D. B.; Li, X.; Cundiff, S. T.; Nelson, K. A. *Science* **2009**, *324*, 1169−1173.

(45) Deria, P.; Sinks, L. E.; Park, T.-H.; Tomezsko, D. M.; Brukman, M. J.; Bonnell, D. A.; Therien, M. J. *Nano Lett.* **2010**, *10*, 4192−4199.

(46) Kang, Y. K.; Lee, O.-S.; Deria, P.; Kim, S. H.; Park, T.-H.; Bonnell, D. A.; Saven, J. G.; Therien, M. J. *Nano Lett.* **2009**, *9*, 1414−1418.

(47) Deria, P.; Von Bargen, C. D.; Olivier, J.-H.; Kumbhar, A. S.; Saven, J. G.; Therien, M. J. *J. Am. Chem. Soc.* **2013**, *135*, 16220−16234.

(48) Blackburn, J. L.; Holt, J. M.; Irurzun, V. M.; Resasco, D. E.; Rumbles, G. *Nano Lett.* **2012**, *12*, 1398−1403.

(49) Vora, P. M.; Tu, X.; Mele, E. J.; Zheng, M.; Kikkawa, J. M. *Phys. Rev. B* **2010**, *81*, 155123.

(50) Tretiak, S. *Nano Lett.* **2007**, *7*, 2201−2206.

(51) Habenicht, B. F.; Prezhdo, O. V. *J. Am. Chem. Soc.* **2012**, *134*, 15648−15651.

(52) Korovyanko, O. J.; Sheng, C.-X.; Vardeny, Z. V.; Dalton, A. B.; Baughman, R. H. *Phys. Rev. Lett.* **2004**, *92*, 17403.

(53) Manzoni, C.; Gambetta, A.; Menna, E.; Meneghetti, M.; Lanzani, G.; Cerullo, G. *Phys. Rev. Lett.* **2005**, *94*, 207401.

(54) Huang, L.; Krauss, T. D. *Phys. Rev. Lett.* **2006**, *96*, 57407.

(55) Valkunas, L.; Ma, Y.-Z.; Fleming, G. R. *Phys. Rev. B* **2006**, *73*, 115432.

(56) Graham, M. W.; Chmeliov, J.; Ma, Y.-Z.; Shinohara, H.; Green, A. A.; Hersam, M. C.; Valkunas, L.; Fleming, G. R. *J. Phys. Chem. B* **2011**, *115*, 5201−5211.

(57) Heller, D. A.; Mayrhofer, R. M.; Baik, S.; Grinkova, Y. V.; Usrey, M. L.; Strano, M. S. *J. Am. Chem. Soc.* **2004**, *126*, 14567−14573.

(58) Huang, X.; Mclean, R. S.; Zheng, M. *Anal. Chem.* **2005**, *77*, 6225−6228.

(59) Miyauchi, Y.; Matsuda, K.; Yamamoto, Y.; Nakashima, N.; Kanemitsu, Y. *J. Phys. Chem. C* **2010**, *114*, 12905−12908.

(60) Hertel, T.; Himmelein, S.; Ackermann, T.; Stich, D.; Crochet, J. *ACS Nano* **2010**, *4*, 7161−7168.

(61) Larsen, B. A.; Deria, P.; Holt, J. M.; Stanton, I. N.; Heben, M. J.; Therien, M. J.; Blackburn, J. L. *J. Am. Chem. Soc.* **2012**, *134*, 12485−12491.

(62) Rosario-Canales, M. R.; Deria, P.; Therien, M. J.; Santiago-Avilés, J. J. *ACS Appl. Mater. Interfaces* **2012**, *4*, 102−109.

(63) Bonhommeau, S.; Deria, P.; Glesner, M. G.; Talaga, D.; Najjar, S.; Belin, C.; Auneau, L.; Trainini, S.; Therien, M. J.; Rodriguez, V. *J. Phys. Chem. C* **2013**, *117*, 14840−14849.

(64) Tsyboulski, D. A.; Bachilo, S. M.; Kolomeisky, A. B.; Weisman, R. B. *ACS Nano* **2008**, *2*, 1770−1776.

(65) Cognet, L.; Tsyboulski, D. A.; Rocha, J. D. R.; Doyle, C. D.; Tour, J. M.; Weisman, R. B. *Science* **2007**, *316*, 1465−1468.

(66) Pimenta, M. A.; Jorio, A.; Brown, S. D. M.; Souza Filho, A. G.; Dresselhaus, G.; Hafner, J. H.; Lieber, C. M.; Saito, R.; Dresselhaus, M. S. *Phys. Rev. B* **2001**, *64*, 041401.

(67) Dillon, A. C.; Parilla, P. A.; Alleman, J. L.; Gennett, T.; Jones, K. M.; Heben, M. J. *Chem. Phys. Lett.* **2005**, *401*, 522−528.